Chapter 2

Origin of Piezoelectricity in Piezoelectric Ceramics from the Viewpoints of Elastic Constants Measured by Acoustic Wave Velocities

Toshio Ogawa

Additional information is available at the end of the chapter

http://dx.doi.org/10.5772/60793

Abstract

This chapter consists of two parts; the first part describes *"how can high piezoelectricity be realized from measuring acoustic wave velocities?"* That is, the measurement of sound velocities resulted in an effective tool for researching and developing piezoelectric materials, and, furthermore, it was possible to design the material compositions of lead-free piezoelectric ceramics as well as lead-containing ceramics. The second part describes the *"effects of firing and DC poling treatments on elastic constants measured from acoustic wave velocities in barium titanate piezoelectric ceramics"*. Namely, it could be applied to manufacturing processes such as firing and DC poling treatments in piezoelectric ceramics, which is accompanied with densification of ceramics and ferroelectric domain aligment, respectively. It is clarified through the two parts that the evaluation of elastic constants leads to the origin of piezoelectricity in piezoelectric ceramics.

Keywords: origin of piezoelectricity, piezoelectric ceramics, acoustic wave velocities, elastic constants, domain alignment

1. Introduction

1.1. How can high piezoelectricity be realized from measuring acoustic wave velocities?

Lead-free piezoelectric ceramics have been studied by many researchers [1-4], because of replacing Pb(Zr, Ti)O_3 (PZT) ceramics. There are three major chemical compositions: alkali niobate [5], alkali bismuth titanate [6], and barium titanate [7]. While relatively high piezoelectricity is realized in alkali niobate (the piezoelectric strain d_{33} constant is 307 pC/N in 0.95(Na, K, Li, Ba)$(Nb_{0.9}Ta_{0.1})O_3$-0.05$SrZrO_3$ with a small amount of MnO [5, 8]) and barium titanate, low piezoelectricity with low dielectric constant and high mechanical quality factor is obtained in alkali bismuth titanate.

Improving the piezoelectricity in lead-free ceramics, a study on Young's modulus (Y) vs. piezoelectricity is important how to realize higher piezoelectricity in piezoelectric materials. We have already reported Y in PZT [9-13], $PbTiO_3$ (PT) [14], $BaTiO_3$ (BT) [7], alkali niobate ceramics composed of (Na, K, Li, Ba)$(Nb_{0.9}Ta_{0.1})O_3$-$SrZrO_3$ (SZ) [5, 8] and in a relaxor single crystal of Pb$[(Zn_{1/3}Nb_{2/3})_{0.91}Ti_{0.09}]O_3$ (PZNT) [15-17] by measuring the impedance responses in various kinds of piezoelectric resonators. Figure 1 shows the relationships between Y and electromechanical coupling factors of transverse mode (k_{31}) and longitudinal mode (k_{33}) in piezoelectric materials. From these figures, it is clarified that the decrease in Y increased the piezoelectricity such as k_{31} and k_{33}, because materials with lower Y were easy to deform by DC poling field. Therefore, it is said that the measurement of Y was important to obtain high piezoelectricity.

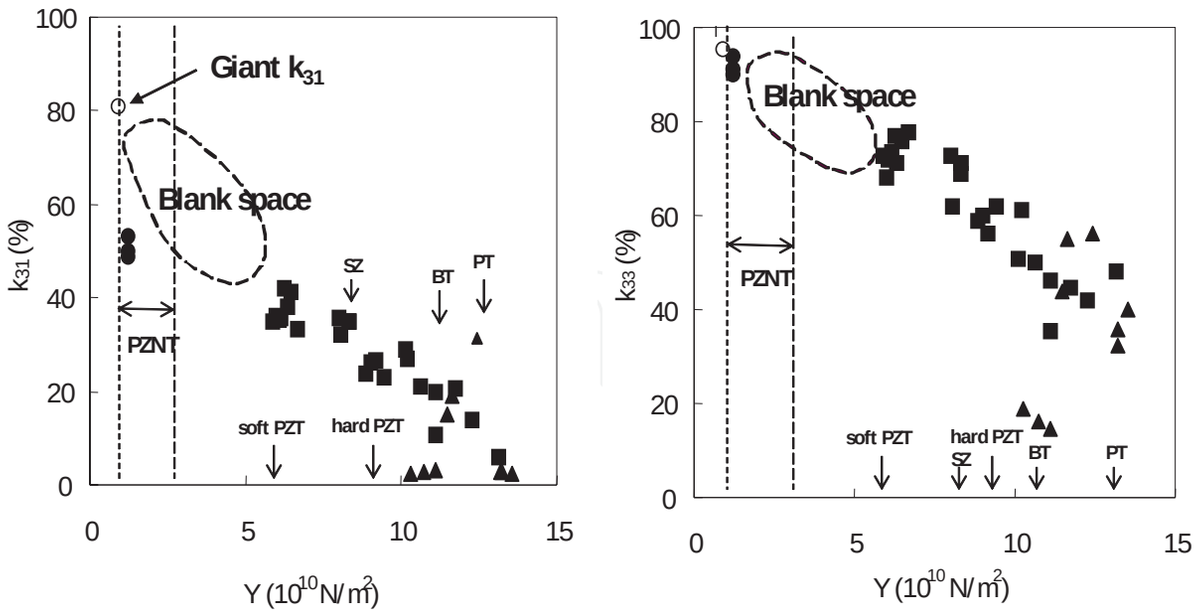

Figure 1. Relationships between Young's modulus (Y) and coupling factors of transverse mode (k_{31}) and longitudinal mode (k_{33}) in piezoelectric ceramics and relaxor single crystals; giant k_{31} was realized in Pb$[(Zn_{1/3}Nb_{2/3})_{0.91}Ti_{0.09}]O_3$ (PZNT) single-crystal plate and there is blank space for coupling factors in the range of Y = 1 – 5 × 10^{10} N/m^2; PZT, PT, BT, and SZ mean Pb(Zr, Ti)O_3, $PbTiO_3$, $BaTiO_3$, and alkali niobate, respectively.

http://dx.doi.org/10.5772/60793

Recently, we developed a novel method to easily measure acoustic wave velocities suitable for conventional disk samples with ordinary dimensions (10-20 mm diameter and 0.5-2.0 mm thickness) by an ultrasonic thickness gauge with high-frequency pulse oscillation [18-20]. Therefore, this method was applied to hard and soft PZT [9-13, 21] and lead-free ceramics composed of alkali niobate [5, 8] and alkali bismuth titanate [6]. In this pursuit, we report the acoustic wave velocities in piezoelectric ceramics measured by our developed method and the calculation results of Young's modulus, Poisson's ratio, modulus of rigidity and bulk modulus, especially to obtain high piezoelectricity in lead-free ceramics. Furthermore, we propose the design for R&D on piezoelectric materials from a viewpoint of measuring acoustic wave velocities.

1.2. Experimental procedure

The piezoelectric ceramic compositions measured were as follows: $0.05Pb(Sn_{0.5}Sb_{0.5})O_3$-$(0.95-x)PbTiO_3$-$xPbZrO_3$ (x = 0.33, 0.45, 0.48, 0.66, 0.75) with (hard PZT) and without 0.4 wt% MnO_2 (soft PZT) [9-13, 21]; $0.90PbTiO_3$-$0.10La_{2/3}TiO_3$ (PLT) and $0.975PbTiO_3$-$0.025La_{2/3}TiO_3$ (PT) [14]; $(1-x)(Na, K, Li, Ba)(Nb_{0.9}Ta_{0.1})O_3$-$xSrZrO_3$ (SZ) (x = 0.00, 0.02, 0.04, 0.05, 0.06, 0.07) [5, 8]; $(1-x)(Na_{0.5}Bi_{0.5})TiO_3$ (NBT)-$x(K_{0.5}Bi_{0.5})TiO_3$ (KBT) (x = 0.08, 0.18) and 0.79NBT-0.20KBT-$0.01Bi(Fe_{0.5}Ti_{0.5})O_3$ (BFT) (x = 0.20) [6]; and $(1-x)$NBT-$xBaTiO_3$ (BT) (x = 0.03, 0.07, 0.11) [6].

DC poling was conducted for 30 minutes at the most suitable poling temperature (T_P) depending on the Curie points of the ceramic materials. The DC poling field (E) depended on the coercive fields and the insulation resistance of the piezoelectric ceramics. The DC poling conditions are as follows: E = 3, 000 V/mm and T_P = 150 ℃ for SZ; E = 2, 500-3, 000 V/mm and T_P = 70 ℃ for KBT and BT; E = 3, 000 V/mm and T_P = 80 ℃ for hard and soft PZT; E = 4, 000 V/mm and T_P = 80 ℃ for PLT; E = 4, 000 V/mm and T_P = 200 ℃ for PT, respectively. Before and after DC poling, the dielectric and piezoelectric properties were measured at room temperature using an LCR meter (HP4263A), a precision impedance analyzer (Agilent 4294A), and a piezo-d_{33} meter (Academia Sinica ZJ-3D). Furthermore, the acoustic wave velocities were measured using an ultrasonic precision thickness gauge (Olympus 35DL), which has PZT transducers with 30 MHz for longitudinal wave (V_L) generation and 20 MHz for transverse wave (V_S) generation [22]. The acoustic wave velocities were evaluated on the basis of the propagation time between the second-pulse echoes in the thickness of ceramic disks parallel to the poling field with dimensions of 14 mm diameter and 0.5-1.5 mm thickness [18-20]. The sample thickness was measured using a precision micrometer (Mitutoyo MDE-25PJ). The number (n) of disk samples measured was n = 5-8, and the data in the figures indicate the average of individual measured values. In addition, Young's modulus (Y), Poisson's ratio (σ), modulus of rigidity (G), and bulk modulus (K) in the thickness direction of ceramic disks were calculated on the basis of the V_L and V_S, as shown in the following equations [23, 24]:

$$Y = 3\rho V_S^2 \frac{V_L^2 - \frac{4}{3}V_S^2}{V_L^2 - V_S^2} \quad (1)$$

$$\sigma = \frac{1}{2}\left\{1 - \frac{1}{\left(\frac{V_L}{V_S}\right)^2 - 1}\right\} \tag{2}$$

$$G = \rho V_S^2 \tag{3}$$

$$K = \rho\left(V_L^2 - \frac{4}{3}V_S^2\right) \tag{4}$$

where ρ is the bulk density of the ceramic disks. Figure 2 shows the relationships between the ratio of sound velocities (V_S/V_L), the elastic constants, and dielectric and piezoelectric constants.

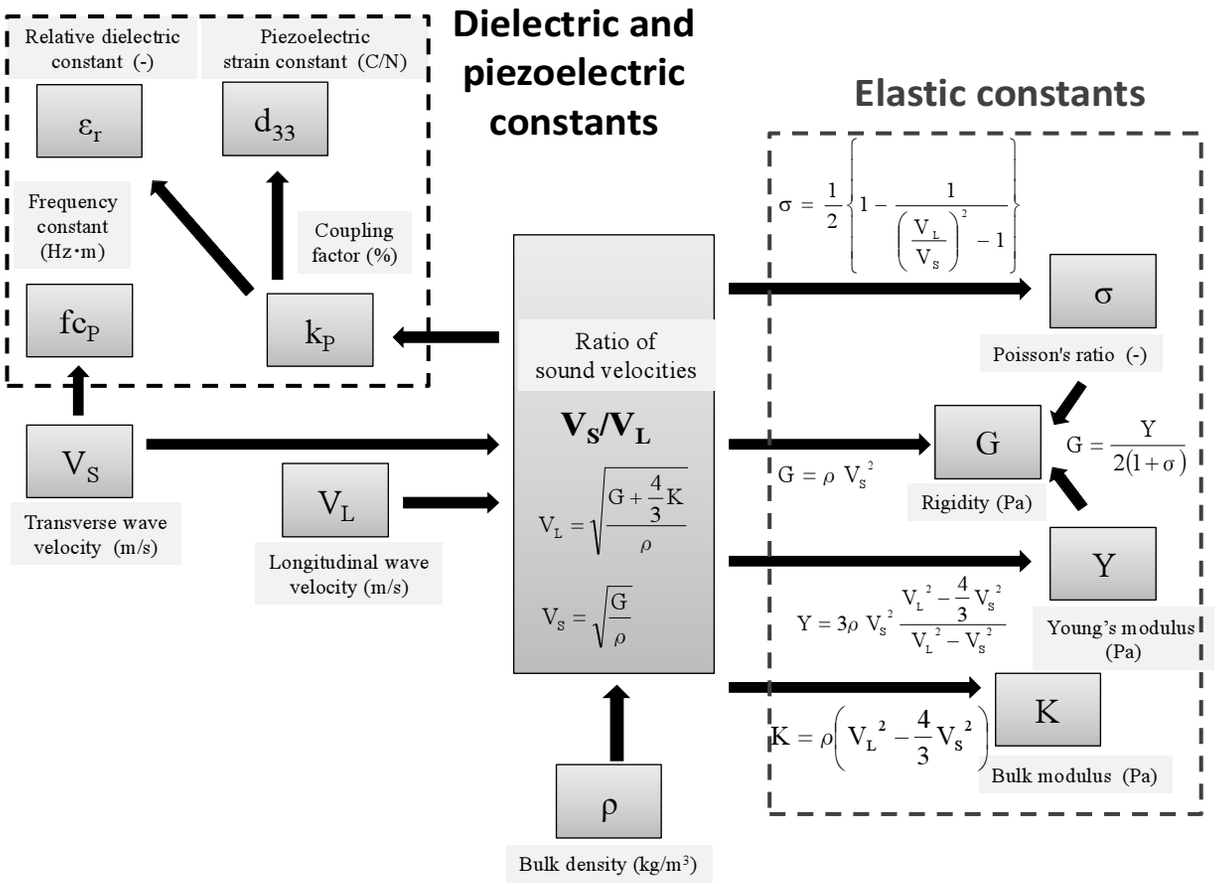

Figure 2. Relationships between the ratio of sound velocities (V_S/V_L), elastic constant and dielectric and piezoelectric constants.

1.3. Results and discussion

1.3.1. Dependence of planar coupling factor on elastic constant

Figure 3 shows the relationships between longitudinal (V_L) and transverse (V_S) wave velocities, Young's modulus (Y), Poisson's ratio (σ), modulus of rigidity (G), and bulk modulus (K) vs. planar coupling factors (k_p) of disk in (1- *x*)(Na, K, Li, Ba)($Nb_{0.9}Ta_{0.1}$)O_3-*x*SZ (abbreviated to "SZ"), (1-*x*)NBT-*x*KBT ("KBT"), 0.79NBT-0.20KBT-0.01BFT ("KBT"), and (1-*x*)NBT-*x*BT ("BT") lead-free ceramics compared with 0.05Pb($Sn_{0.5}Sb_{0.5}$)O_3-(0.95-*x*)$PbTiO_3$-*x*$PbZrO_3$ ceramics with ("hard PZT") and without 0.4 wt% MnO_2 ("soft PZT"), and with 0.90$PbTiO_3$-0.10$La_{2/3}TiO_3$ ("PLT") and 0.975$PbTiO_3$-0.025$La_{2/3}TiO_3$ ("PT") ceramics before and after fully DC poling. In the case of after poling (marks and solid lines in Figure 3), although the V_L values of the PZT ceramics were almost constant at approximately 4, 600-4, 800 m/s independently of the composition *x*, their V_S values linearly decreased from 2, 500 to 1, 600 m/s with increasing k_p from 20% to 65% (solid line). In addition, the V_L and V_S values of the PZT ceramics were smaller than those of the lead-free ceramics (V_L = 5, 000-5, 800 m/s and V_S = 2, 600-3, 000 m/s; solid lines). Although the V_L values of the PT ceramics were almost the same (4, 800 m/s) as those of the PZT ceramics, the V_S values of the PT ceramics were approximately 2, 700 m/s. On the other hand, the V_L values of the SZ ceramics were relatively high (5, 500-5, 800 m/s); furthermore, the V_S values of the SZ ceramics also increased (2, 600-2, 700 m/s) and linearly decreased with increasing k_p from 25% to 50% (solid line), the behavior of which was almost the same as that of the V_S values of the PZT ceramics. The V_L values of the KBT, BT, and PLT ceramics (5, 000-5, 400 m/s) were between those of the PZT, PT, and SZ ceramics. However, the V_S values of the KBT, BT, and PLT ceramics (2, 800-3, 000 m/s) were the highest. Therefore, it was possible to divide V_L and V_S into three material groups, namely, PZT and PT/ KBT, BT (alkali bismuth titanate), and PLT/ SZ (alkali niobate). In addition, k_p increased from 4% to 65% with decreasing Y from 15 × 10^{10} to 6 × 10^{10} N/m^2 and increased with increasing σ from 0.25 to 0.43. It was clarified that higher k_p values can be realized at lower Y and G, and higher σ and K.

In comparison with the values of before poling (the k_p was made use of the values after poling; marks and dash lines in Figure 3), V_L, σ, and K increase and V_S, Y, and G decrease after poling because of ferroelectric domain alignment. In addition, while the correlation coefficients in the k_p vs. Y, σ, and G were almost independent of poling treatment, the coefficients in the k_p vs. K after poling increases from 0.49 to 0.74. It is thought that the increase in K is significant to realize piezoelectricity as mentioned below.

Figure 4 shows the relationships between k_p vs. changes (Δ) in longitudinal (V_L) and transverse wave velocities (V_S) [$\Delta V_L/\Delta V_S$], and changes in Young's modulus (Y), Poisson's ratio (σ), bulk modulus (K), and rigidity (G) [$\Delta Y/\Delta\sigma/\Delta K/\Delta G$] before and after DC poling in soft and hard PZT, $PbTiO_3$ (PT/PLT), alkali niobate (SZ), and alkali bismuth titanate (KBT/ BT). Higher k_p was realized in the regions of large $+\Delta V_L$ and $+\Delta K$, and larger $-\Delta V_S$, $-\Delta Y$, and $-\Delta G$. There were thresholds regarding k_p vs. ΔV_S, ΔY, and ΔG around -5%, -7%, and -10%, respectively. On the other hand, there were no thresholds in the cases of k_p vs. ΔV_L and ΔK, especially $\Delta\sigma$. As there were k_p peaks regarding $\Delta\sigma$ in hard and soft PZT ceramics and k_p maximum in alkali niobate (SZ) ceramics, the compositions in k_p peaks and k_p maximum correspond to a morphotropic phase boundary (MPB) in PZT [25] and to take lowest value of V_S/V_L in SZ (see the following

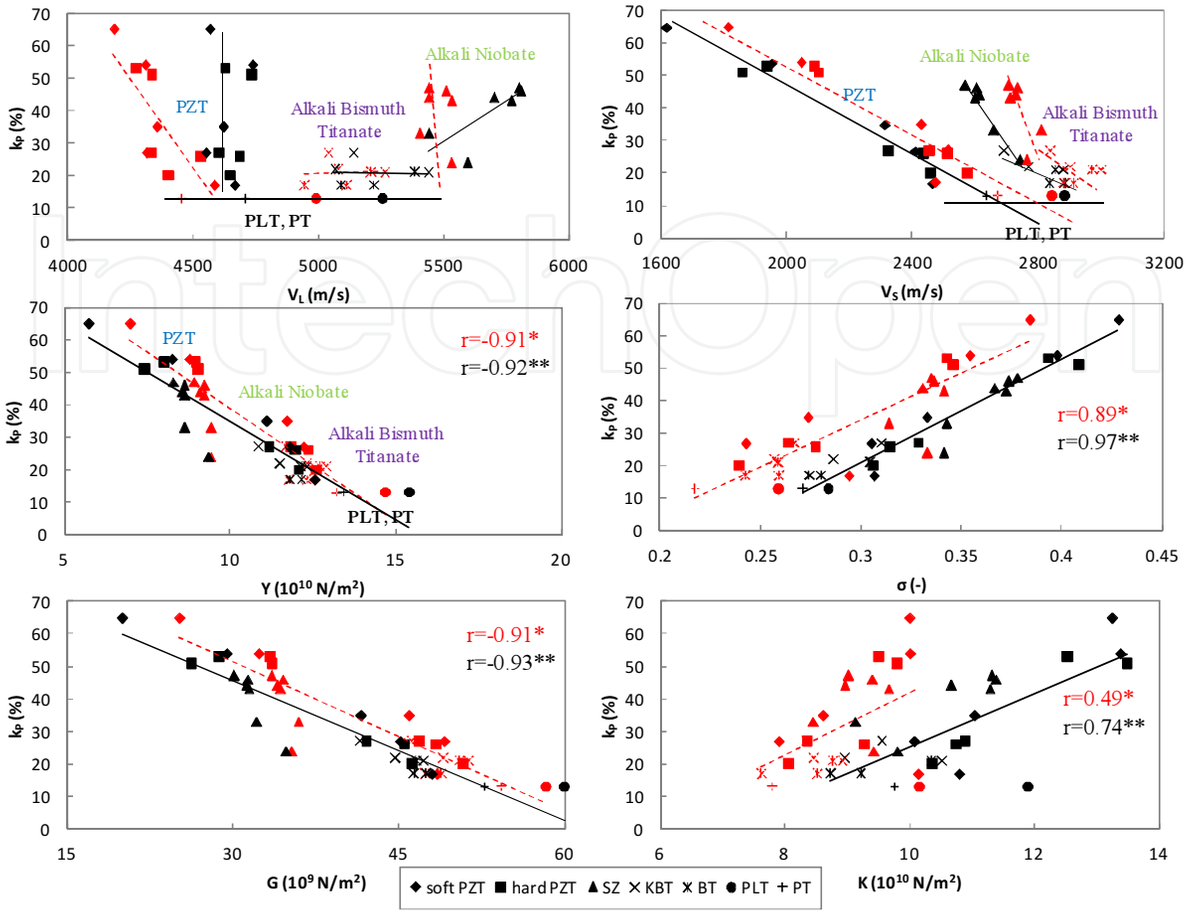

Figure 3. V_L, V_S, Y, σ, G, and K vs. k_p before* (red marks, dash lines) and after poling** (black marks, solid lines) in lead-containing and lead-free ceramics (r: correlation coefficient).

Figure 10). We believe that the origin of piezoelectricity in piezoelectric ceramics was due to large change in V_S ($-\Delta V_S$) while applying DC poling field parallel to the thickness of disks. Therefore, the larger changes in V_S ($-\Delta V_S$) correspond to larger changes in Y ($-\Delta Y$) and G ($-\Delta G$). These phenomena mean that the origin of high piezoelectricity was due to the mechanical softness of the materials under compress stress (large $+\Delta V_L$ and $+\Delta K$). In addition, the realization of high piezoelectricity is easy deformation by DC poling field in diameter (large $-\Delta G$) as well in thickness (large $-\Delta Y$).

Figure 5 shows schematic charts between domain alignment and the changes in Y, σ, G, and K after DC poling. Comparing domain alignment before poling to the alignment after poling, same charges (+ or -) are generated and gathered in the regions of each ends by opposite charge due to DC poling field, namely orientation polarization which occurs by domain alignment. The orientation polarization acts by reducing of Y and G by repulsion to each other because there are same charges in domain alignment. The enhancing σ and K can be explained by the same phenomena. Therefore, it can be said that higher domain alignment leads to large changes in Y, G, and K. However, large change in σ ($+\Delta\sigma$ in Figure 4) does not lead to higher domain alignment since σ value is decided by the combinations of Y (G) and K after poling.

http://dx.doi.org/10.5772/60793

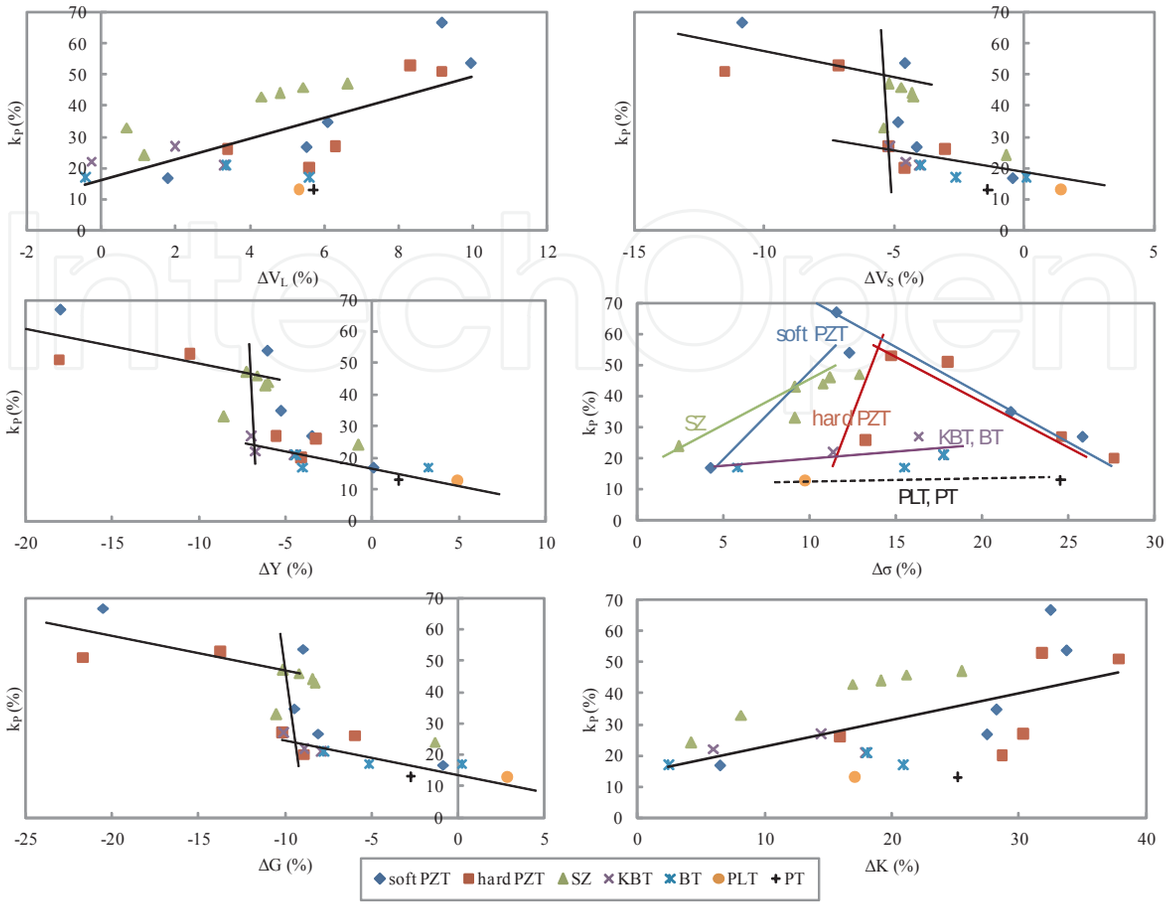

Figure 4. Changes (Δ) in V_L, V_S, Y, σ, G, and K vs. k_p before and after poling in lead-containing and lead-free ceramics.

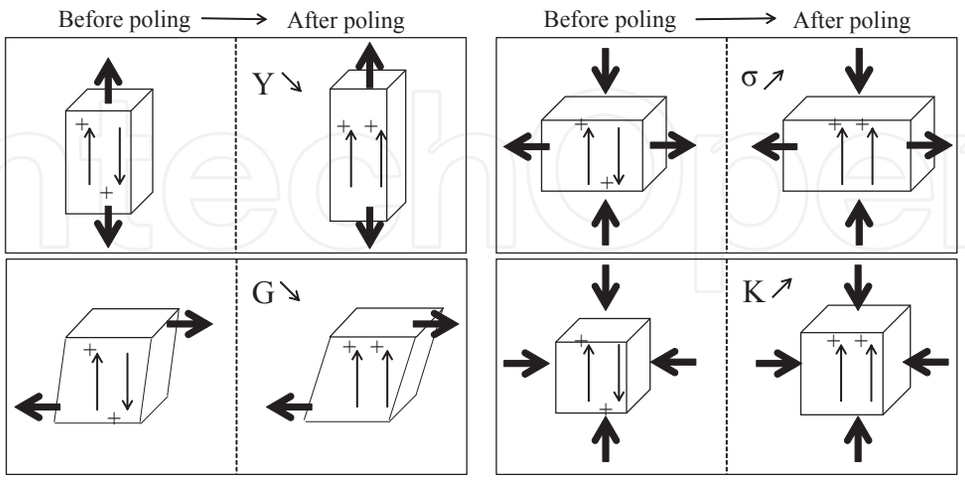

Figure 5. Effect of ferroelectric domain alignment by DC poling on Y, σ, G, and K; generated charges (- → +) accompanied with domain alignments, displacement (→) and changes in Y, σ, G, and K (↘: decrease, ↗: increase) after poling are also shown in this figure.

1.3.2. Design for research and development on lead-free piezoelectric ceramics

Figure 6 shows the relationship between V_S/V_L vs. k_p. The k_p linearly increased with decreasing V_S/V_L in lead-free ceramics as well as lead-containing ceramics such as PZT, PLT, and PT. Furthermore, it was confirmed that V_S/V_L was an effective figure to evaluate both the elastic constants and the piezoelectric constants.

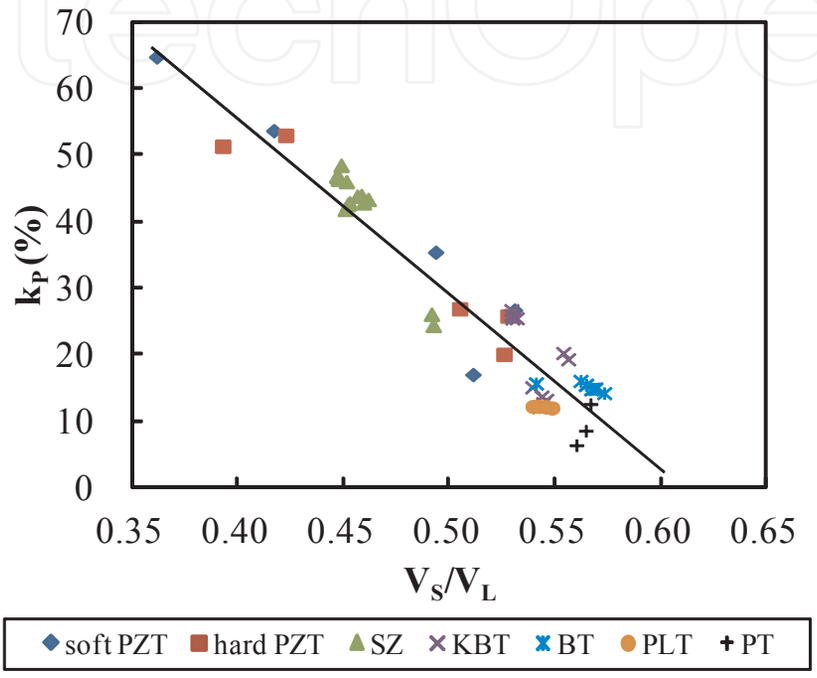

Figure 6. Relationship between ratio of sound velocities (V_S/V_L) and planar coupling factor (k_p) in lead-free and lead-containing ceramics.

When we research and develop new piezoelectric ceramics with high piezoelectricity in lead-free ceramics, we must need a new concept different from the conventional research looking for chemical compositions such as MPB [25]. From the equations (1)-(4) and the change in V_L and V_S before and after poling as mentioned previously (Figure 4), we focused on the ceramic bulk density (ϱ). Figure 7 shows the relationship V_S/V_L vs. ϱ: ϱ of lead-containing ceramics (PZT, PLT, and PT) was independent of V_S/V_L. However, in lead-free ceramics (SZ, KBT, and BT) ϱ decreased with decreasing V_S/V_L. In the case of ϱ vs. k_p in Figure 8, although k_p in lead-containing ceramics (PZT, PLT, and PT) is independent of V_S/V_L, k_p in lead-free ceramics (SZ, KBT, and BT) increased with decreasing ϱ. From the above results, we came to an important concept to obtain lead-free ceramics with high piezoelectricity, namely the R&D on lead-free ceramics with lower bulk density. As a result, it confirmed the importance of measuring V_L and V_S to evaluate the piezoelectricity.

It was said that the direction of the R&D on lead-free piezoelectric ceramics with high piezoelectricity was looking for ceramics with lower bulk density. For example, in perovskite structure, small cations at A and B sites in perovskite structure of ABO_3 were selected. In

http://dx.doi.org/10.5772/60793

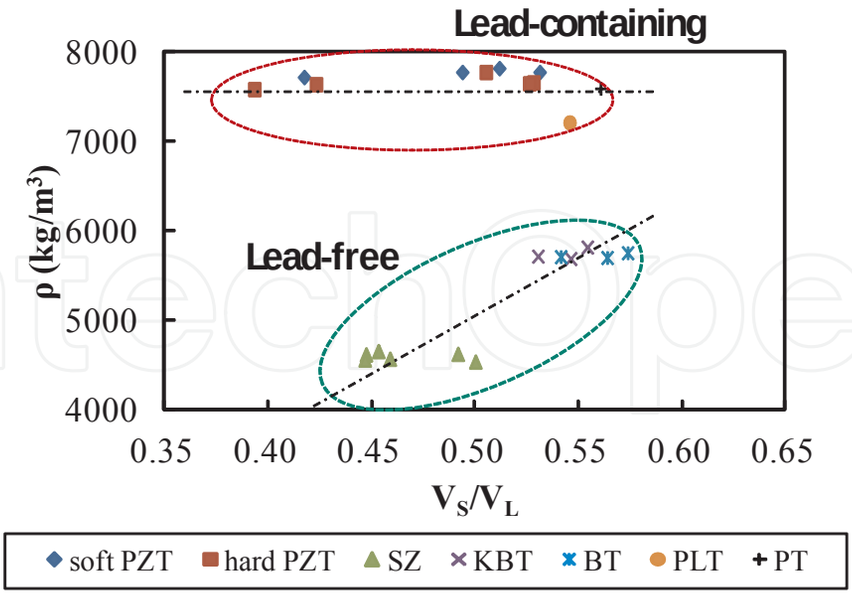

Figure 7. Relationship between ratio of sound velocities (V_S/V_L) and ceramic bulk density (ϱ) in lead-free and lead-containing ceramics.

addition, for practical use, the Curie point (Tc) or depolarization temperature must be over 250 ℃. From the two items we will expect the candidates for new lead-free ceramics such as $SrTeO_3$ (ϱ = 4.82 g/cm³, Tc = 485 ℃) and $YMnO_3$ (Tc = 640 ℃), in addition to $KNbO_3$ (ϱ = 4.62 g/cm³, Tc = 418 ℃) and $LiNbO_3$ (ϱ = 4.46 g/cm³, Tc = 1, 210 ℃), respectively [26, 27]. In fact, the bulk density (ϱ) of SZ, which possessed the highest k_p [5, 8] in lead-free ceramics we investigated, was around 4.6 g/cm³.

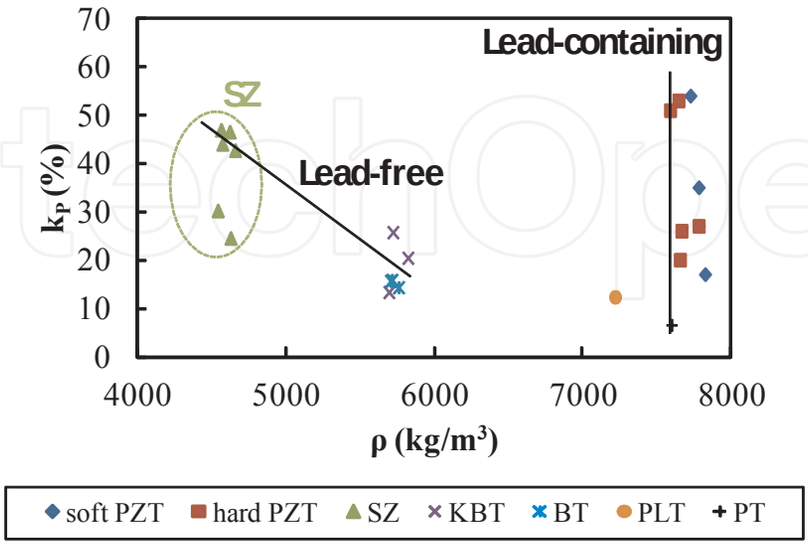

Figure 8. Relationship between ceramic bulk density (ϱ) and planar coupling factor (k_p) in lead-free and lead-containing ceramics.

1.3.3. Ferroelectricity in almost same ceramic bulk density

In addition to the relationships between V_S/V_L vs. k_p in Table 1, we evaluated the chemical composition dependence of V_S/V_L in piezoelectric ceramics. Figure 9 shows the composition x dependence of k_p and d_{33} in (1-x)(Na, K, Li, Ba)$(Nb_{0.9}Ta_{0.1})O_3$-xSrZrO$_3$ (SZ) (x = 0.00, 0.02, 0.04, 0.05, 0.06, 0.07). While the k_p in SZ compositions of x = 0.00 - 0.07 was independent of ϱ in Figure 8, the maximum k_p and d_{33} were obtained at x = 0.04 and 0.05, respectively (Figure 9). Figure 10 shows the x dependence of V_S/V_L in SZ before and after poling. The minimum V_S/V_L after poling were obtained at x = 0.04 - 0.05. From both figures, it was concluded that the highest k_p appeared in the case of the minimum V_S/V_L. However, there is a composition without MPB at x = 0.04 - 0.05 in SZ [5, 8]. Therefore, we could introduce the novel method to evaluate the piezoelectricity by measuring acoustic wave velocities of V_L and V_S in spite of the existence of MPB.

	Lead-free	Lead-containing
Longitudinal wave velocity (V_L)	V_L↗ k_P↗	V_L; independent of k_P
Transverse wave velocity (V_S)	V_S↘ k_P↗	V_S↘ k_P↗
V_S/V_L	V_S/V_L↘ k_P↗	V_S/V_L↘ k_P↗
Ceramic bulk density (ρ)	V_S/V_L↘ ρ↘ ρ↘ k_P↗	ρ; independent of V_S/V_L and k_p

Table 1. Relationships between longitudinal wave velocity (V_L), transverse wave velocity (V_S), ratio of sand velocities (V_S/V_L), ceramic bulk density (ϱ), and planar coupling factor (k_p) in lead-free and lead-containing ceramics.

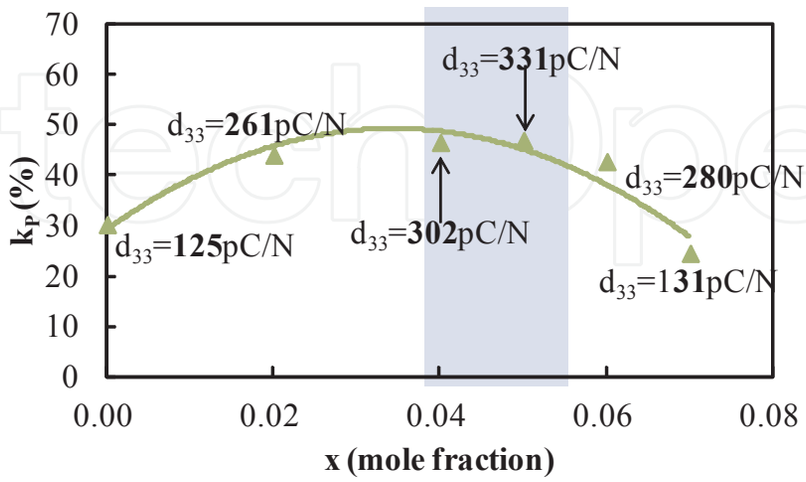

Figure 9. Composition x dependence of k_p and d_{33} in (1–x)(Na, K, Li, Ba)$(Nb_{0.9}Ta_{0.1})O_3$-xSrZrO$_3$ (SZ) (x = 0.00, 0.02, 0.04, 0.05, 0.06, 0.07).

http://dx.doi.org/10.5772/60793

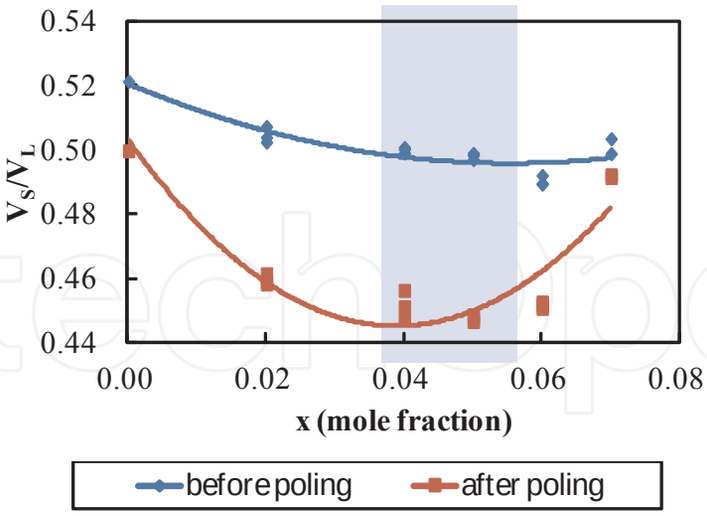

Figure 10. Composition x dependence of ratio of sound velocities (V_S/V_L) in (1–x)(Na, K, Li, Ba)($Nb_{0.9}Ta_{0.1}$)O_3-$x$$SrZrO_3$ (SZ) (x = 0.00, 0.02, 0.04, 0.05, 0.06, 0.07).

We applied this novel method to 0.05Pb($Sn_{0.5}Sb_{0.5}$)O_3-(0.95-x)$PbTiO_3$-$x$$PbZrO_3$ (x = 0.33, 0.45, 0.48, 0.66, 0.75) with (hard PZT) and without 0.4 wt% MnO_2 (soft PZT) to confirm the effectiveness of our developed V_S/V_L evaluation. While k_p in PZT compositions of x = 0.33 - 0.75 was independent of ϱ in Figure 8, the maximum k_p was obtained at MPB around x = 0.45 - 0.48 [11, 21]. Figure 11 shows the x dependence of V_S/V_L in PZT before and after poling. The minimum V_S/V_L before and after poling appeared around x = 0.45 - 0.48. From the relationships between x vs. k_p and V_S/V_L, it was concluded that the highest k_p was realized in the case of minimum V_S/V_L. These compositions around x = 0.45 - 0.48 correspond to MPB in hard and soft PZT. Therefore, it was said that we could introduce the novel method to evaluate the piezoelectricity by measuring acoustic wave velocities of V_L and V_S in the compositions with MPB.

1.3.4. Relationship between the ratio of transverse wave velocity to longitudinal wave velocity and Poisson's ratio

Figure 12 shows the relationship between V_S/V_L vs. σ in solids including piezoelectric ceramics. The equation between σ, V_L, and V_S is shown in this figure. All of the σ in solids was plotted on a line of the equation. The V_S/V_L regions of Poisson's ratio in soft PZT, hard PZT, lead-free and $PbTiO_3$ (PLT and PT) were also shown in this figure. The regions of σ regarding V_S/V_L increased from $PbTiO_3$, lead-free, hard PZT to soft PZT with increasing piezoelectricity. In addition to higher Poisson's ratio, it was clarified that higher k_p can be realized in lager K as shown in Figure 3. We believe the physical meaning of this behavior toward σ is as follows: increasing mechanical softness (lower Y) in piezoelectric materials, it becomes easy to deform by DC poling field. The σ becomes larger while the materials become softer, and furthermore, the K must become larger in order to transmit effectively from longitudinal deformation (the directions of poling and applying electric field are thickness direction of disk) to transverse deformation (the radial direction of disk). In this study, it was described a road map in

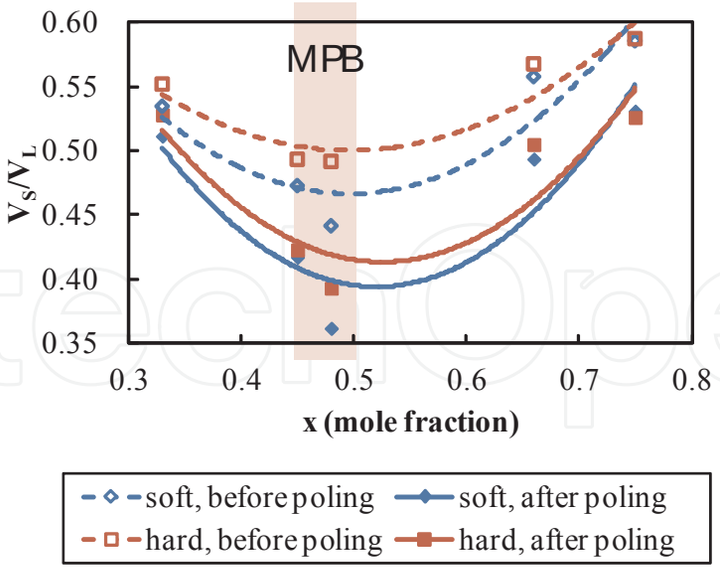

Figure 11. Composition x dependence of ratio of sound velocities (V_S/V_L) in $0.05Pb(Sn_{0.5}Sb_{0.5})O_3$-$(0.95–x)PbTiO_3$-$xPbZrO_3$ (x = 0.33, 0.45, 0.48, 0.66, 0.75) with (hard PZT) and without 0.4 wt% MnO_2 (soft PZT) ceramics before and after poling.

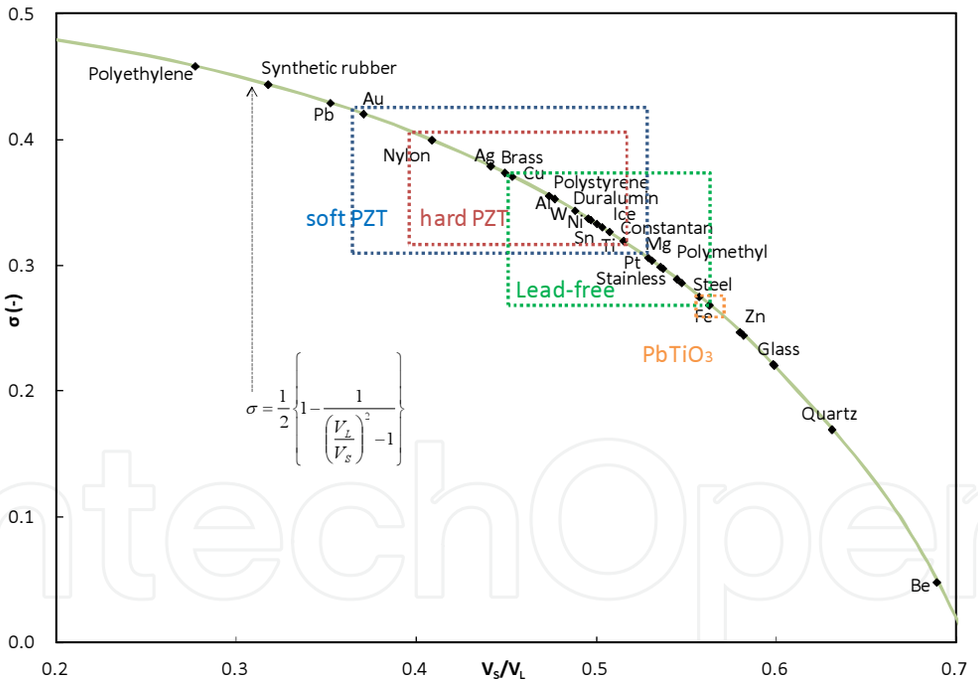

Figure 12. Relationship between ratio of sound velocities (V_S/V_L) and Poisson's ratio (σ) in solids including piezoelectric ceramics.

piezoelectric ceramics regarding the relationships between longitudinal and transverse wave velocities, Young's modulus, Poisson's ratio, modulus of rigidity and bulk modulus to research and develop new piezoelectric ceramic materials, especially lead-free ceramics with high piezoelectricity.

http://dx.doi.org/10.5772/60793

1.4. Conclusions in this part

Longitudinal and transverse wave velocities in PZT, lead titanate, and lead-free ceramics were measured by an ultrasonic precision thickness gauge with high-frequency pulse generation to calculate elastic constants such as Young's modulus, Poisson's ratio, and so forth. Since the ceramic bulk density was focused on to improve piezoelectricity in lead-free ceramics, the candidates of lead-free ceramic compositions with high piezoelectricity were proposed. It was confirmed that our evaluation method was an effective tool for R&D on piezoelectric material. Furthermore, the origin of piezoelectricity in piezoelectric ceramics could be explained by the elastic constants before and after DC poling.

2. Effects of firing and DC poling treatments on elastic constants measured from acoustic wave velocities in barium titanate piezoelectric ceramics

2.1. Introduction

Recently, we have developed a method to evaluate elastic constants, such as Young's modulus and Poisson's ratio, by measuring longitudinal and transverse wave velocities using an ultrasonic thickness gauge with high-frequency generation in comparison with a conventional method [28]. This method has been confirmed to be useful for measuring ceramic disks with diameters of 10-20 mm and thicknesses of 0.5-2.0 mm. In addition, it has been clarified that this method is suitable for evaluating cases involving (1) firing process analysis, such as the analysis of the effect of lead oxide (PbO) atmosphere during firing on the dielectric and piezoelectric properties of lead zirconate titanate (PZT) ceramics, and the oxygen atmosphere firing of PZT ceramics to realize pore-free ceramics, (2) DC poling process analysis, such as the analysis of the DC poling field dependence in as-fired (before poling) ceramics and relaxor single crystals, and (3) piezoelectric materials research and development (R&D) for lead-free ceramics with high piezoelectricity from the viewpoints of elastic constants [18-20].

In this part, to clarify the effects of firing temperature and DC poling on barium titanate (BT) piezoelectric ceramics, we studied the firing temperature and DC poling dependences on acoustic wave velocities and dielectric and piezoelectric properties of BT ceramics. Here, we report the relationships between firing temperature and DC poling effect vs. acoustic wave velocities, Young's modulus, Poisson's ratio, modulus of rigidity, and bulk modulus.

2.2. Experimental procedure

The BT raw materials in this study were utilized for two types of powder particle with high purities above 99.95% and average particle sizes of 0.2 μm (abbreviated to BT02) and 0.5 μm (BT05) (Sakai Chemical Industry). After firing at 1, 300-1, 350 ℃ for BT02 and at 1, 300-1, 360 ℃ for BT05 for 2 h, the bulk density (ϱ) and microstructure of the obtained ceramic disks were evaluated. DC poling was conducted at a temperature of 60 ℃ and a field of 2.0 kV/mm for 30 min. After DC poling, dielectric and piezoelectric properties were measured at room temperature using an LCR meter (HP4263A), a precision impedance analyzer (Agilent 4294A), and a

piezo-d_{33} meter (Academia Sinica ZJ-3D). Furthermore, the acoustic wave velocities of the BT ceramics before and after poling were measured using an ultrasonic precision thickness gauge (Olympus 35DL), which has PZT transducers with a frequency of 30 MHz for longitudinal wave generation and a frequency of 20 MHz for transverse wave generation. The acoustic wave velocities were evaluated on the basis of the propagation time between the second-pulse and the third-pulse echoes in the thickness direction parallel to the DC poling field for the ceramic disks with 14 mm diameter and 0.9-1.2 mm thickness [18-20]. The sample thickness was measured using a precision micrometer (Mitutoyo MDE-25PJ). The number (n) of disk samples measured was n = 5-8, and the data in the figures indicate the average of individual measured values. Furthermore, Young's modulus (Y), Poisson's ratio (σ), modulus of rigidity (G), and bulk modulus (K) in the thickness direction of ceramic disks were calculated on the basis of the longitudinal (V_L) and transverse (V_S) wave velocities using the equations (1)-(4) in Section 1.2. We investigated the relationships between firing temperature and DC poling effect vs. V_L, V_S, Y, σ, G, and K; furthermore, we clarified the relationships between ϱ, the microstructure, and the elastic constants.

2.3. Results and discussion

2.3.1. Firing temperature dependence of dielectric and piezoelectric properties

Figures 13(a)-(d) show the relationships between firing temperature (F_T) and (a) relative dielectric constant (ε_r), (b) planar coupling factor (k_p) for the radial mode on the disks, (c) frequency constant (fc_p), and (d) piezoelectric strain d_{33} constant in the cases of BT02 and BT05 ceramics before and after DC poling. Although ε_r decreases with increasing F_T, k_p, fc_p, and d_{33} with increasing F_T; furthermore, there is an optimum F_T of 1, 340 ℃ in BT02 for obtaining the highest k_p and d_{33}. The differences in the dielectric and piezoelectric properties vs. F_T between BT02 and BT05 were due to the ceramic bulk density, as mentioned later (see the following Figure 17), and the powder particle activity during firing because the specific surface areas of BT02 and BT05 powder particles measured by the Brunauer, Emmett, and Teller (BET) method were 9.4 and 2.3 m^2/g, respectively.

2.3.2. Effects of firing temperature and DC poling on acoustic wave velocities and elastic constants

Figures 14(a)-(d) show the relationships between F_T and (a) longitudinal wave velocity (V_L), (b) transverse wave velocity (V_S), (c) Young's modulus (Y), and (d) Poisson's ratio (σ) in the cases of BT02 and BT05 ceramics. Although V_L, V_S, and Y before and after DC poling increase with increasing F_T, σ after poling is almost independent of F_T; furthermore, there is an optimum F_T of 1, 340 ℃ in BT02 from the plots of F_T vs. V_L and Y. The increase in Y with increasing F_T indicates the increase in the mechanical hardness of the ceramic disks. By comparing F_T vs. V_L in Figure 14(a) with F_T vs. $2fc_p$ (fc_p is shown in Figure 13(c), the dependences of V_L and $2fc_p$ on F_T were almost the same, because both of them correspond to longitudinal wave velocities, as shown in Figure 15. In addition, we confirmed that V_L precisely corresponded to $2fc_t$, which is twice the frequency constant (fc_t) of the coupling factor (k_t) for the thickness mode on the disks measured using the typical impedance vs. frequency response (Figure 15) [29].

Therefore, it is considered that our measurement method using the ultrasonic precision thickness gauge is suitable for evaluating acoustic wave velocities, especially in piezoelectric ceramics.

Figures 16(a)-(b) show the changes in Y (ΔY) and σ (Δσ) during poling, respectively. ΔY decreases with increasing F_T, regardless of the types of BT powder particle. This phenomenon indicates that the ceramics become mechanically softer after DC poling. It is considered that such a change is due to the ferroelectric domain (↑) alignment induced by the poling field, such as a change in the configuration from a random orientation (↑ ↓) before poling to a directional orientation (↑ ↑) after poling [5-7, 9-15]. Δσ abruptly increases from F_T of 1, 320 ℃ and shows almost the same tendency as in the case of F_T vs. k_p in Figure 13(b). By comparing F_T vs. k_p (Figure 13(b)) with F_T vs. Δσ (Fig. 16(b)), a higher k_p was obtained in the case of a larger Δσ. The physical meaning of the phenomenon regarding σ was deduced, that is, a larger Δσ was needed to realize a higher k_p because of the easy deformation of the bulk perpendicular to the poling field (radial direction in the disks) as well as parallel to the poling field (thickness direction in the disks).

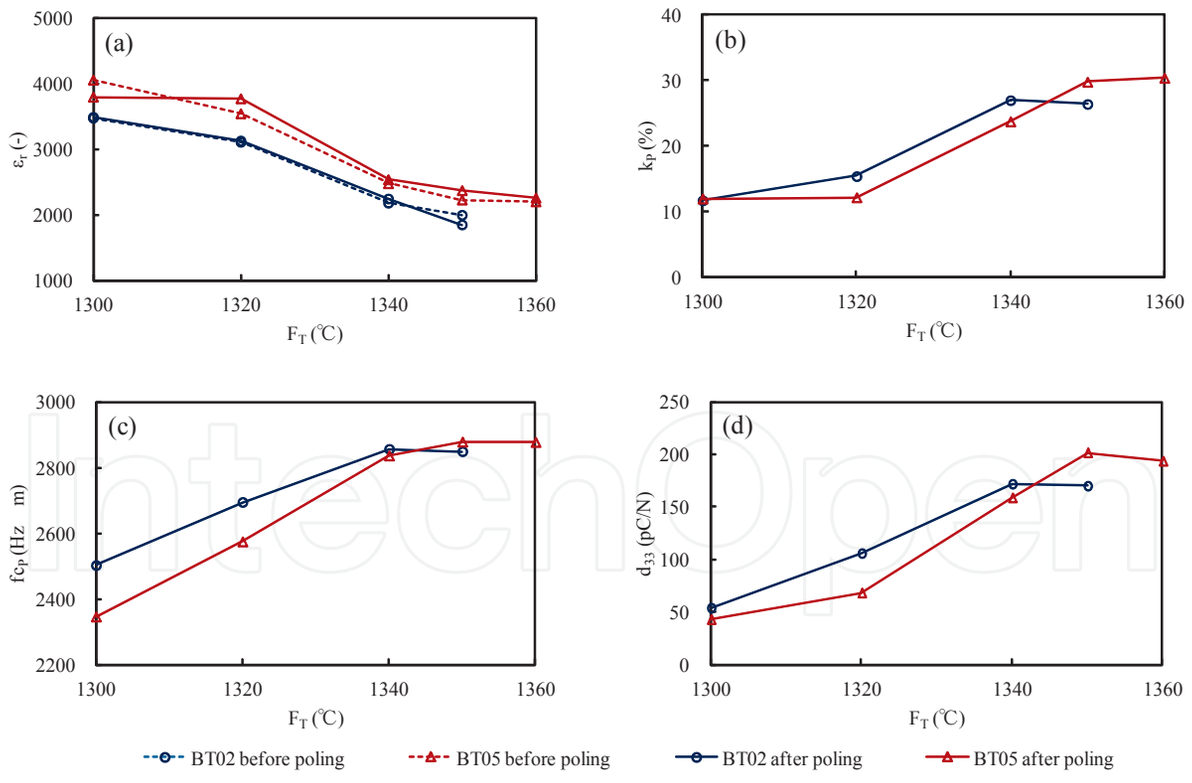

Figure 13. Firing temperature (F_T) vs. (a) relative dielectric constant (ε_r), (b) planar coupling factor (k_p) for radial mode on disks, (c) frequency constant (fc_p), and (d) piezoelectric strain d_{33} constant in BT02 and BT05 ceramics before and after DC poling.

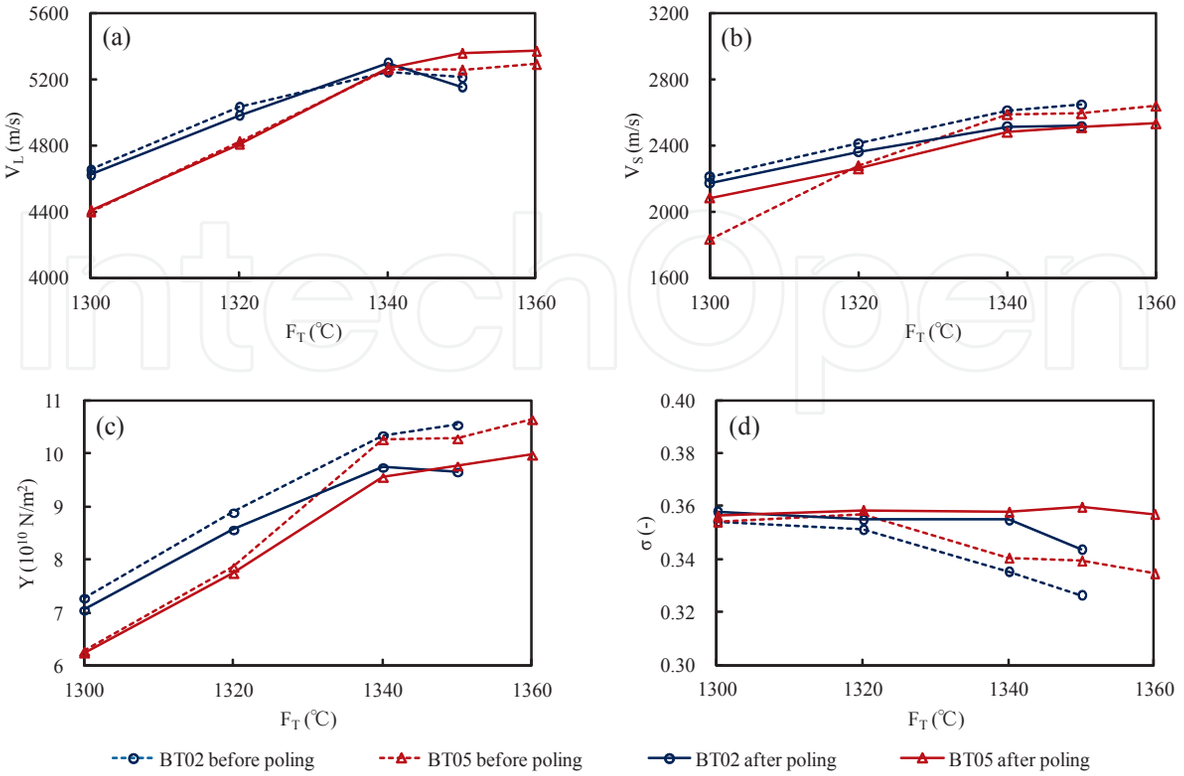

Figure 14. Firing temperature (F_T) vs. (a) longitudinal wave velocity (V_L), (b) transverse wave velocity (V_S), (c) Young's modulus (Y), and (d) Poisson's ratio (σ) in BT02 and BT05 ceramics before and after DC poling.

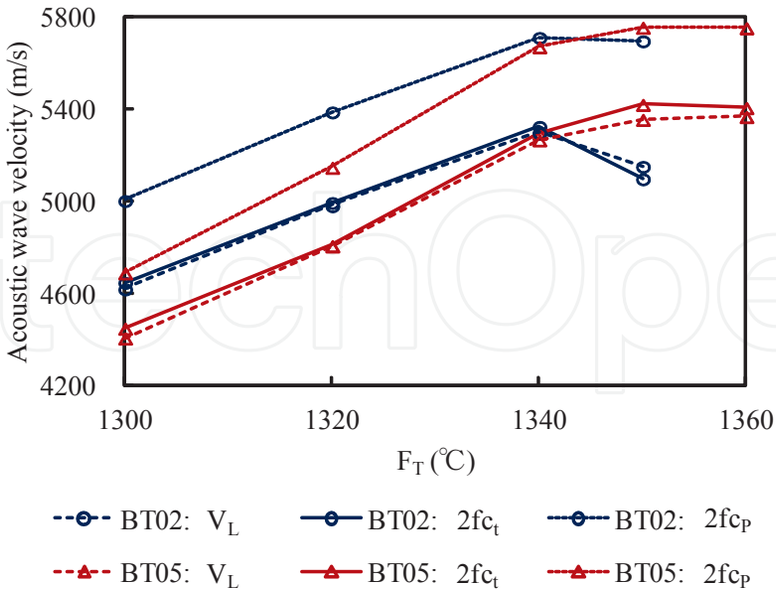

Figure 15. Comparison between longitudinal wave velocity (V_L), $2fc_t$, and $2fc_P$, which are twice the frequency constants of fc_t for the thickness mode and fc_p for the radial mode on disks in BT02 and BT05 ceramics after DC poling; $2fc_t$ and $2fc_p$ correspond to acoustic wave velocities.

http://dx.doi.org/10.5772/60793

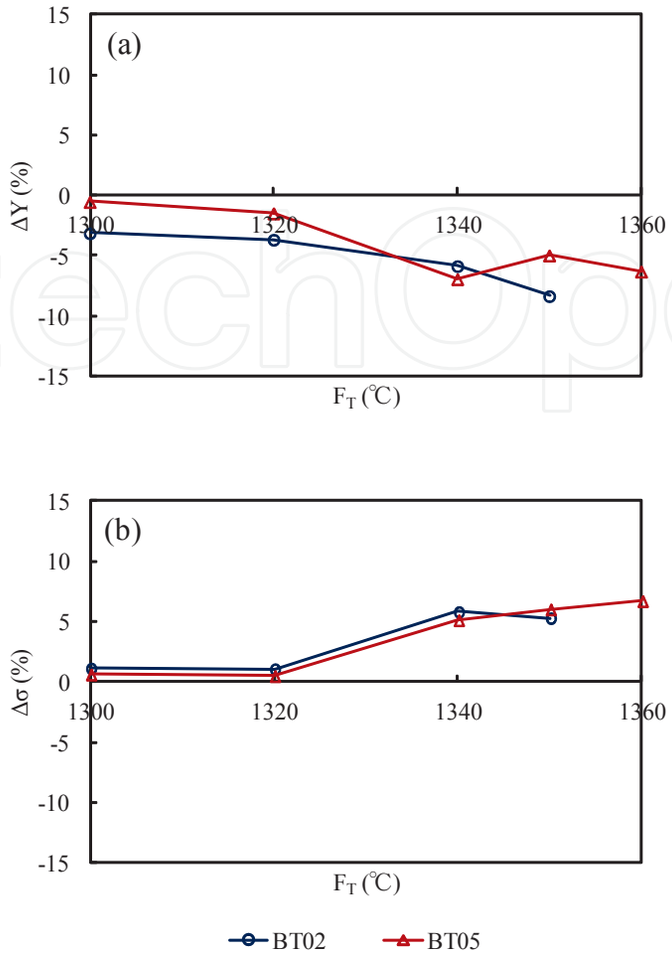

Figure 16. Changes in (a) Young's modulus (ΔY) and (b) Poisson's ratio (Δσ) in BT02 and BT05 ceramics during DC poling.

2.3.3. Relationship between ceramic microstructure and elastic constants

Figure 17 shows the F_T dependence of the bulk density (ϱ) of the ceramic disks. The relative bulk density (ϱ/ϱ_0) became over 94% for both BT02 and BT05 during firing at 1, 340-1, 360 ℃, where ϱ_0 (6.02 g/cm^3) is the theoretical density of BT ceramics [25]. From our previous study on the relationships between k_p vs. Y and σ in piezoelectric ceramics, a higher k_p was realized at a lower Y and a higher σ [18-20]. However, there is no correspondence between the lower Y (Fig. 14(c)), the higher σ (Fig. 14(d)), the lower k_p (Fig. 13(b)), and the lower d_{33} (Fig. 13(d)) during firing at 1, 300-1, 320 ℃ because of the low relative bulk density of ϱ/ϱ_0 (< 0.94). On the other hand, while Y became almost constant during firing at 1, 340-1, 360 ℃ (Fig. 14(c)), σ before poling decreased with increasing F_T (Fig. 14(d)). It was considered that the decrease in σ with increasing F_T was due to the increase in the density of coarse grains with average diameters of 50 μm as mentioned later. As F_T vs. σ before poling (Fig. 14(d)) shows the same tendency as F_T vs. ε_r (Fig. 13(a)), the ε_r of which is directly related to ferroelectric domain structures, the σ dependence of F_T was considered to be due to the domain structures and anisotropy of coarse

grains being different from those of fine grains with average diameters of 1.2 μm. Since the ferroelectric domain size increases with increasing grain size of BT ceramics, the domain density decreases in the case of coarse grains [30-33]. Therefore, the ceramics with coarse grains exhibit a lower ε_r and a larger crystal anisotropy than the ceramics with fine grains [34-38]. Furthermore, σ decreases with increasing F_T because it approaches a behavior similar to that of a BT single crystal, σ of which is 0.29 while σ of the ceramics is 0.31 [25]. In order to evaluate the physical characteristics of ceramic grains, the modulus of rigidity (G) and bulk modulus (K) were calculated by the equations (3) and (4) in Section 1.2. [23, 24]: G and K before poling increase with increasing F_T during firing at 1,300-1,360 ℃, as shown in Figures 18(a)-(b), respectively, because the ceramic bulk density is improved in BT ceramics as shown in Figure 17; as a result, G and K are obtained from the equations (3) and (4), as well as Y in Figure 14(c) from equation (1). On the other hand, σ is independent of the ceramic bulk density, as shown in equation (2). Figures 19(a)-(d) show the relationships between ϱ/ϱ_0 vs. Y, σ, G, and K, respectively. Y, G, and K depend on ϱ/ϱ_0 because they are affected by increasing the mechanical strength, especially the hardness of the ceramics, with F_T. As mentioned previously regarding Figure 14(d), σ is independent of ϱ/ϱ_0 except when ϱ/ϱ_0 is above 0.94, as shown in Figure 19(b), which corresponds to ceramics with a larger domain size and a lower domain density with coarse grains. G decreased and K increased after poling owing to the domain alignment as shown in Figure 18. In addition, the change in G (ΔG) in BT ceramics during poling linearly decreased with increasing F_T, and peaks of the changes in K (ΔK), which correspond to the peaks of $\Delta\sigma$ (Figure 16(b)), were obtained at F_T of 1340 ℃ in the BT02 ceramics and at F_T of 1, 350-1, 360 ℃ in the BT05 ceramics, as shown in Figures 20(a)-(b). Therefore, a higher k_p could be realized at F_T at the peaks of ΔK and $\Delta\sigma$. Since ceramic grains with a higher K due to domain alignment during DC poling, indicating a high ceramic bulk density for obtaining a higher k_p, are difficult to change in terms of their volume while applying external stress, the deformation of grains is practically transferred from the parallel direction to the perpendicular direction toward the direction of the applied stress; as a result, a higher σ is achieved. We believe that the increase in σ ($\Delta\sigma$) as a result of the increase in K (ΔK) indicates fundamental issues regarding the poling of ceramic grains to obtain a higher k_p; therefore, the R&D of piezoelectric ceramics with high piezoelectricity must be focused on to realize a lower G and a higher K during DC poling from the viewpoints of elastic constants. From the above-mentioned results, it was considered that the values of F_T vs. G and K in BT02 and BT05 ceramics after poling (Figures 18(a)-(b)) correspond to the values of k_p vs. F_T (Figure 13(b)).

Figure 21(a) shows the F_T dependence of microstructures in the BT02 ceramics. With the increase in k_p with F_T, ceramic grains grew from 1.2 μm (fine grains shown as white parts in the figures) to 50 μm (coarse grains shown as black parts in the figures) in diameter; moreover, the ratio of black parts to whole parts (black parts plus white parts) increased. The border between fine and coarse grains is shown in Figures 21(b)-(c). Furthermore, it was found that the black parts consist of several coarse grains, as shown in Figure 21(b). This phenomenon was almost the same as in the case of the microstructure in the BT05 ceramics. Figure 22 shows the relationship between k_p and the area ratio of coarse grains (black parts) measured by image-analyzing software (WinROOF [39]). In this figure, when the area ratio increases, k_p increases because of the increase in the density of coarse grains. Therefore, the coarse grains in the dense

http://dx.doi.org/10.5772/60793

ceramic bulk contribute to a higher k_p and V_L, V_S, Y, and σ in the coarse grains correspond to those at F_T of 1, 360 ℃ in Figures 14(a)-(d), which almost agree with the values previously reported [25].

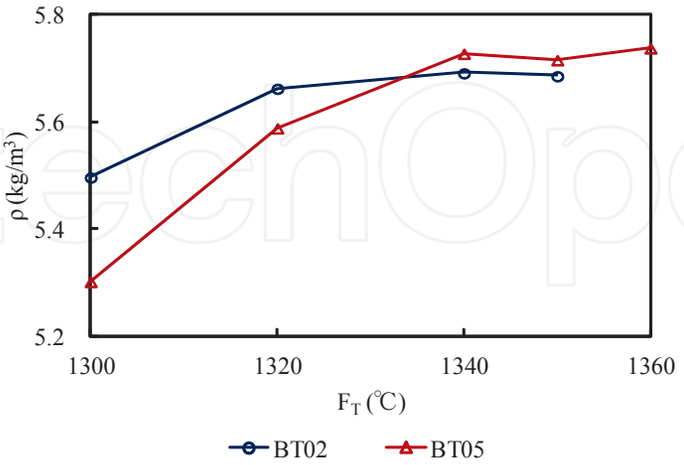

Figure 17. Firing temperature (F_T) dependence of bulk density (ρ) in BT02 and BT05 ceramic disks.

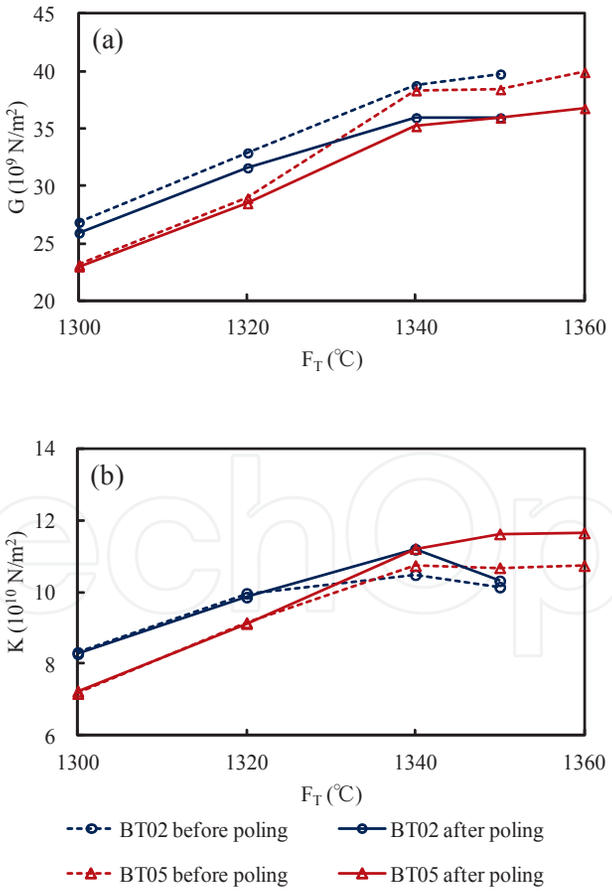

Figure 18. Firing temperature (F_T) vs. (a) modulus of rigidity (G) and (b) bulk modulus (K) in BT02 and BT05 ceramics before and after DC poling.

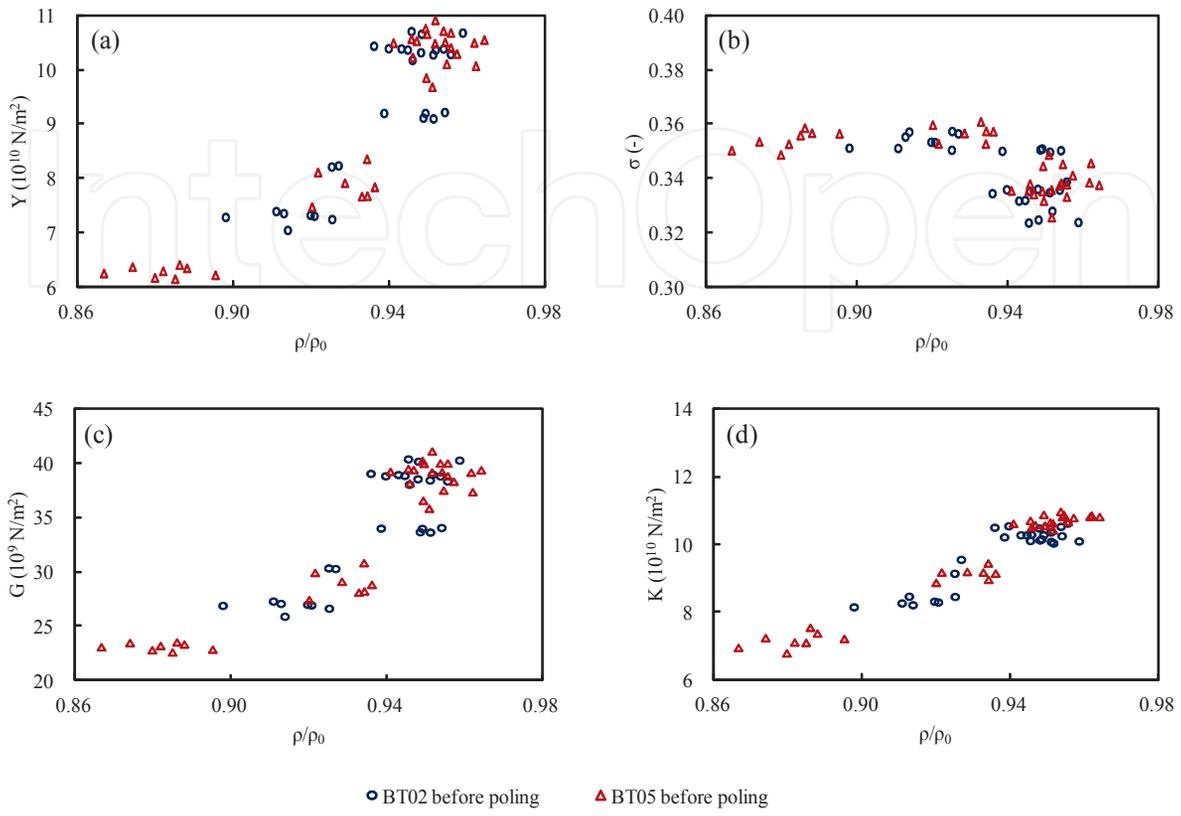

Figure 19. Relative bulk density (ϱ/ϱ_0) dependences of (a) Young's modulus (Y), (b) Poisson's ratio (σ), (c) modulus of rigidity, and (d) bulk modulus (K) in BT02 and BT05 as-fired (before poling) ceramics sintered during firing at 1, 300-, 360 ℃, where ϱ and ϱ_0 (6.02 g/cm^3) are the measured bulk density and theoretical density [25] of BT ceramics, respectively.

2.3.4. Firing temperature dependence of elastic constants in barium titanate ceramics

Figure 23 shows that the relationships between k_p vs. Y, σ, G, and K in BT02 and BT05 ceramics fired at different temperatures were inserted into the relationships between k_p vs. Y, σ, G, and K in lead-containing and lead-free piezoelectric ceramics (Figure 3), which were fired at the optimal temperatures for each composition to realize the maximum k_p. Higher k_p is obtained in the cases of lower Y and G, and furthermore, higher σ and K, which are indicated by yellow arrows in Figure 23. This figure also indicates the firing temperature dependence of the bulk density vs. Y, σ, G, and K in BT02 and BT05 ceramics in Figure 19. k_p increases with the increase of Y, G, and K because of the increase in bulk density with increasing firing temperature. On the other hand, σ was independent of k_p because σ is an intrinsic material constant. These phenomena are indicated by green arrows in Figure 23. It is predicted the same phenomena regarding the firing temperature and bulk density dependences on k_p vs. Y, σ, G, and K in cases of lead-containing and lead-free ceramics.

http://dx.doi.org/10.5772/60793

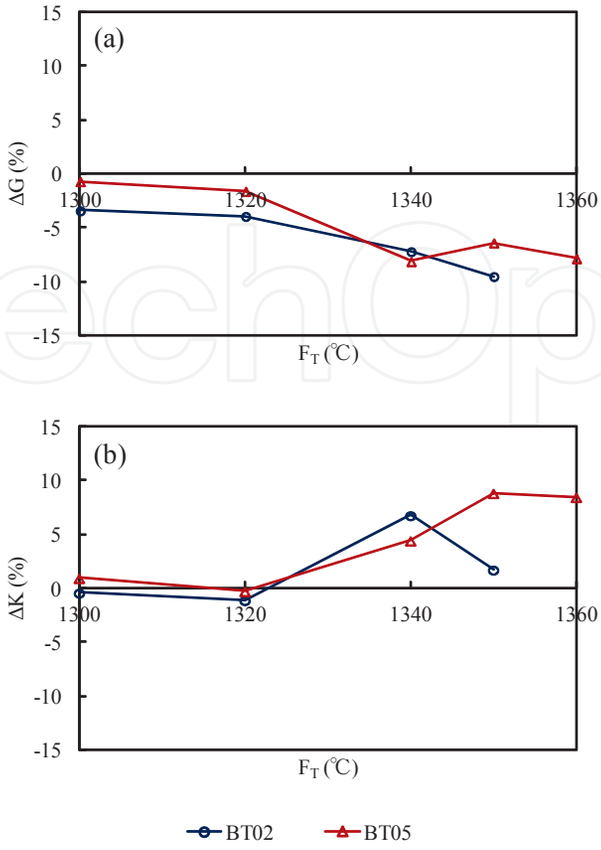

Figure 20. Changes in modulus of rigidity (ΔG) and bulk modulus (ΔK) in BT02 and BT05 ceramics during DC poling.

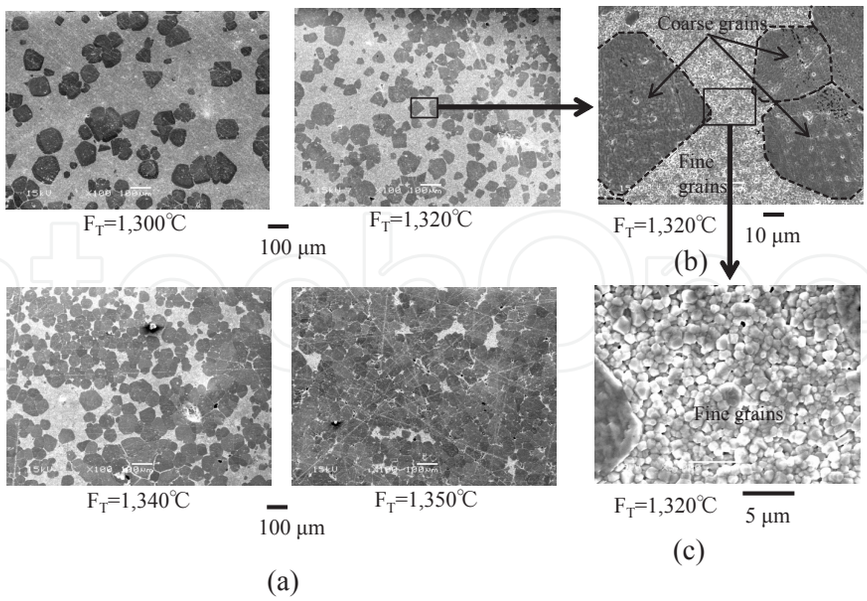

Figure 21. (a) Firing temperature (F_T) dependence of microstructures in BT02 ceramics, (b) border between fine grain [see (c), average grain size of 1.2 μm] and coarse grain [see (b), average grain size of 50 μm], and relationship between black parts and coarse grains.

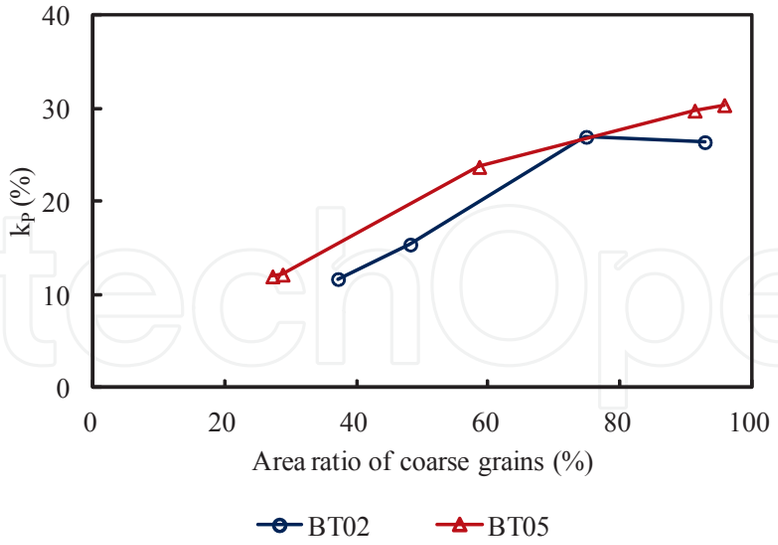

Figure 22. Planar coupling factor (k_p) vs. area ratio of coarse grains of black parts measured by an image-analyzing software program (WinRoof [39]).

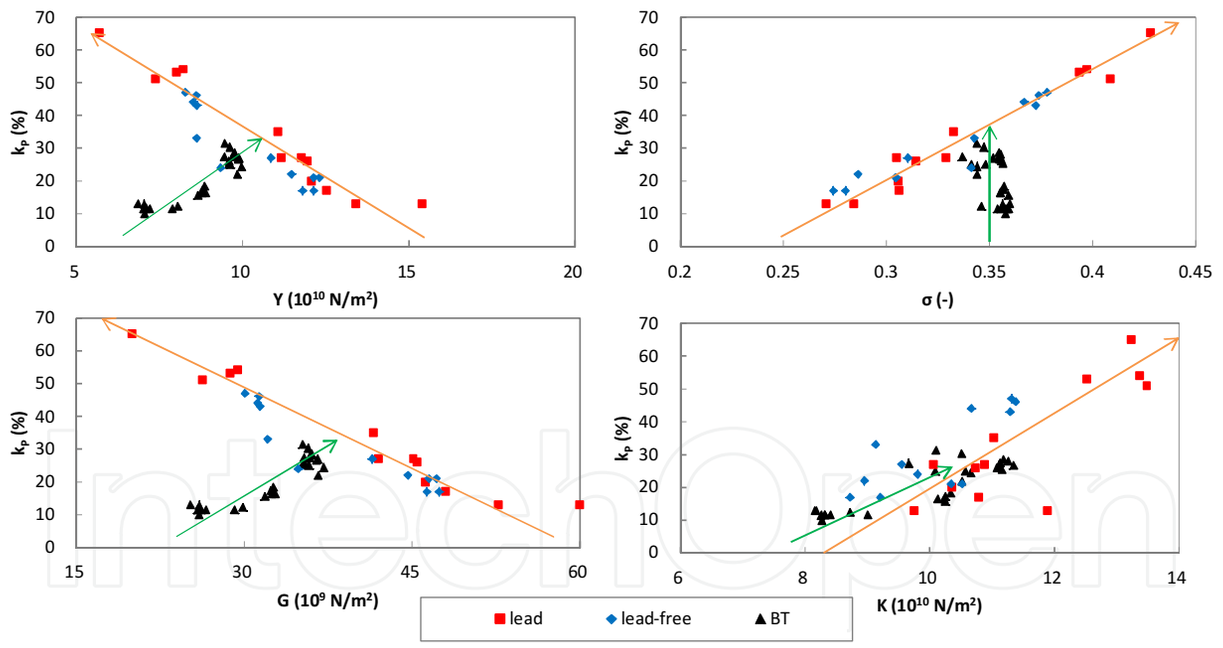

Figure 23. Planar coupling factor (k_p) vs. Y, σ, G, and K in BT02 and BT05 ceramics fired at different temperatures. These data were inserted into the relationships between k_p vs. Y, σ, G, and K in lead-containing and lead-free piezoelectric ceramics (Figure 3), which were fired at the optimal temperatures for each composition to realize maximum k_p.

2.4. Conclusions in this part

The effects of firing temperature and DC poling on the longitudinal and transverse wave velocities in barium titanate ceramics were investigated using an ultrasonic precision thickness

http://dx.doi.org/10.5772/60793

gauge with high-frequency pulse generation. The results could explain the relationships between acoustic wave velocities, Young's modulus, Poisson's ratio, the modulus of rigidity, and the bulk modulus vs. firing temperature, and the changes in elastic constants during DC poling.

3. Summary of this chapter

Sound velocities were evaluated in ceramic disks composed of lead-containing and lead-free ceramics using an ultrasonic precision thickness gauge with high-frequency pulse generation, and furthermore, dielectric and piezoelectric constants were simultaneously measured utilizing the same disk samples. Calculating elastic constants by using the sound velocities, higher piezoelectricity in ceramics were obtained in lower Young's modulus and rigidity, and furthermore, higher Poisson's ratio and bulk modulus. Piezoelectric ceramics with lower Young's modulus and rigidity caused by ferroelectric domain alignment while DC poling were easy to deform by electric field and external force. In addition to these phenomena, higher bulk modulus needs to realize higher Poisson's ratio. Lower Young's modulus means mechanical soft in ceramics; however, higher bulk modulus, which means mechanical hard in ceramics, need to obtain higher piezoelectricity. It was thought that these characteristics run counter to the mechanical characteristics of piezoelectric ceramics; however, it was the origin of piezoelectricity in ceramics.

Acknowledgements

This work was partially supported by two Grants-in-Aid for Scientific Research C (Nos. 21560340 and 26420282), a Grant from the Strategic Research Foundation Grant-Aided Project for Private Universities 2010-2014 (No. S1001032) from the Ministry of Education, Culture, Sports, Science and Technology, Japan (MEXT), and a Cooperation Research Foundation 2014 between Academy and Industry of Fukuroi City, Shizuoka, Japan.

Author details

Toshio Ogawa

Address all correspondence to: ogawa@ee.sist.ac.jp

Department of Electrical and Electronic Engineering, Shizuoka Institute of Science and Technology, Toyosawa, Fukuroi, Shizuoka, Japan

References

[1] Saito Y, Takao H, Tani T, Nonoyama T, Takatori K, Homma T, Nagaya T, Nakamura M. Lead-free piezoceramics. Nature 2004;432:84-7.

[2] Yang ZP, Liu B, Wei LL, Hou YT. Structure and electrical properties of (1-x)$Bi_{0.5}Na_{0.5}TiO_3$-x$Bi_{0.5}K_{0.5}TiO_3$ ceramics near morphotropic phase boundary. Mater Res Bull 2008;43:81-9.

[3] Zhao W, Zhou HP, Yan YK, Liu D. Morphotropic phase boundary study of the BNT-BKT lead-free piezoelectric ceramics. Key Eng Mater 2008;368-372:1908-10.

[4] Dai YJ, Pan JS, Zhang XW. Composition range of morphotropic phase boundary and electrical properties of NBT-BT system. Key Eng Mater 2007;336-338:206-9.

[5] Ogawa T, Furukawa M, Tsukada T. Poling field dependence of piezoelectric properties and hysteresis loops of polarization versus electric field in alkali niobate ceramics. Jpn J Appl Phys 2009;48:709KD07-1-5.

[6] Ogawa T, Nishina T, Furukawa M, Tsukada T. Poling field dependence of ferroelectric properties in alkali bismuth titanate lead-free ceramics. Jpn J Appl Phys 2010;49:09MD07-1-4.

[7] Ogawa T. Poling field dependence of ferroelectric properties in barium titanate ceramics. Jpn J Appl Phys 2001;40:5630-3.

[8] Furukawa M, Tsukada T, Tanaka D, Sakamoto N. Alkaline niobate-based lead-free piezoelectric ceramics. Proc 24th Int Japan-Korea Semin Ceramics 2007;339-42.

[9] Ogawa T, Yamada A, Chung YK, Chun DI. Effect of domain structures on electrical properties in tetragonal PZT ceramics. J Korean Phys Soc 1998;32:S724-S726.

[10] Ogawa T, Nakamura K. Poling field dependence of ferroelectric properties and crystal orientation in rhombohedral lead zirconate titanate ceramics. Jpn J Appl Phys 1998;37:5241-5.

[11] Ogawa T, Nakamura K. Effect of domain switching and rotation on dielectric and piezoelectric properties in lead zirconate titanate ceramics. Jpn J Appl Phys 1999;38:5465-9.

[12] Ogawa T. Domain switching and rotation in lead zirconate titanate ceramics by poling fields. Ferroelectrics 2000;240:75-82.

[13] Ogawa T. Domain structure of ferroelectric ceramics. Ceram Int 2000;25:383-90.

[14] Ogawa T. Poling field dependence of crystal orientation and ferroelectric properties in lead titanate ceramics. Jpn J Appl Phys 2000;39:5538-41.

[15] Ogawa T. Poling field dependence of ferroelectric properties in piezoelectric ceramics and single crystal. Ferroelectrics 2002;273:371-6.

[16] Kato R, Ogawa T. Chemical composition dependence of giant piezoelectricity on k_{31} mode in $Pb(Mg_{1/3}Nb_{2/3})O_3$-$PbTiO_3$ single crystals. Jpn. J. Appl. Phys. 2006;45:7418-21.

[17] Ogawa T. Giant k_{31} relaxor single-crystal plate and their applications. In Lallart M. (ed.) Ferroelectrics –Applications–. Rijeka: Intech; 2011, pp.3-34.

[18] Ogawa T, Nishina T. Acoustic wave velocities measurement on piezoelectric ceramics to evaluate Young's modulus and Poisson's ratio for realization of high piezoelectricity. In Nair KM, Priya S. (eds.) Ceramic Transactions, Advances and Applications in Electroceramics II. Hoboken: Wiley; 2012;235:pp.105-12.

[19] Ogawa T, Ishii K, Matsumoto T, Nishina T. Poling field dependence of longitudinal and transverse wave velocities, Young's modulus, and Poisson's ratio in piezoelectric ceramics. J Appl Phys 2012;51:09LD03-1-5.

[20] Ogawa T. Acoustic wave velocity measurement on piezoelectric ceramics. In Ebrahimi F. (ed.) Piezoelectric Materials and Devices –Practice and Applications–. Rijeka: Intech; 2013, pp.35-52.

[21] Ogawa T. Highly functional and high-performance piezoelectric ceramics. Ceramic Bull 1991;70:1042-9.

[22] Olympus Co. Ultrasonic Precision Thickness Gages User's Manual. Part No. 910-261-EN, Revision H. Waltham: Olympus NDT Inc; 2008.

[23] Mason WP. Piezoelectric Crystals and Their Application to Ultrasonics. Princeton: Nostrand; 1950, p.390.

[24] Philippoff W, Brodnyan J. Preliminary results in measuring dynamic compressibilities. J Appl Phys 1955;26:846.

[25] Jaffe B, Cook WR, Jaffe H. Piezoelectric Ceramics. London: Academic Press; 1971.

[26] Landolt-Bornstein Group III. Condensed Matter, Ferroelectrics and Related Substances. Berlin: Springer; 2001, 36A1.

[27] Landolt-Bornstein Group III. Condensed Matter, Ferroelectrics and Related Substances. Berlin: Springer; 2002, 36A2.

[28] Mason WP. Physical Acoustics. New York: Academic Press; 1964, Part A, p.182.

[29] IEEE Standard. 1988;pp.176-1987.

[30] Salje E. Domain mobilities and elastic instabilities in ferroelastic and co-elastic materials. In Phase Transitions in Ferroelastic and Coelastic Crystals. Cambridge: Cambridge University Press; 1990, p.76.

[31] Arlt G. The influence of microstructure on the properties of ferroelectric ceramics. Ferroelectrics 1990;104:217.

[32] Randall CA, Kim N, Kucera JP, Cao W, Shrout TR. Intrinsic and extrinsic size effects in fine-grained morphotropic-phase-boundary lead zirconate titanate ceramics. J Am Ceram Soc 1988;81:677.

[33] Cao W, Randall CA. Grain size and domain size relations in bulk ceramic ferroelectric materials. J Phys Chem Solids 1996;10:1499.

[34] Arlt G, Hennings D, With GD. Dielectric properties of fine-grained barium titanate ceramics. J Appl Phys 1985;58:1619.

[35] Buessem WR, Cross LE, Goswami AK. Phenomenological theory of high permittivity in fine-grained barium titanate. J Am Ceram Soc 1966;49:33.

[36] Kinoshita K, Yamaji A. Grain-size effects on dielectric properties in barium titanate ceramics. J Appl Phys 1976;47:371.

[37] Arlt G, Peusens H. The dielectric constant of coarse grained $BaTiO_3$ ceramics. Ferroelectrics 1983;48:213.

[38] Demartin M, Damjanovic D. Dependence of the direct piezoelectric effect in coarse and fine grain barium titanate ceramics on dynamic and static pressure. Appl Phys Lett 1996;68:3046.

[39] http://mitani-visual.jp/winroof01.html.